Acta Mechanica Sinica (2019) 35(1):99–111
https://doi.org/10.1007/s10409-018-0804-x

RESEARCH PAPER

Frictionally excited thermoelastic dynamic instability of functionally graded materials

J. Liu[1] · L. L. Ke[2] · Y. S. Wang[2]

Received: 9 April 2018 / Revised: 21 June 2018 / Accepted: 28 July 2018 / Published online: 29 October 2018

Abstract
The perturbation method is applied to investigate the frictionally excited thermoelastic dynamic instability (TEDI) of a functionally graded material (FGM) coating in half-plane sliding against a homogeneous half-plane. We assume that the thermoelastic properties of the FGM vary exponentially with thickness. We also examine the effects of the gradient index, sliding speed, and friction coefficient on the TEDI for various material combinations. The transverse normal stress for two different coating structures is calculated. Furthermore, the frictional sliding stability of two different coating structures is analyzed. The obtained results show that use of FGM coatings can improve the TEDI of this sliding system and reduce the possibility of interfacial failure by controlling the interfacial tensile stress.

Keywords Thermoelastic dynamic instability · Frictional heat · Functionally graded materials · Stress analysis

1 Introduction

The effective material properties of functionally graded materials (FGMs) can change in a continuous and smooth manner, since they are usually formed from two distinct material phases with continuously varying fractions [1]. Over the past 20 years, contact problems involving FGMs have attracted attention from many researchers. The frictional contact problem of an FGM coating structure acted on by rigid parabolic and cylindrical stamps was analyzed by Guler and Erdogan [2–5], whereas El-Borgi et al. [6] and Elloumi et al. [7] investigated the axisymmetric receding contact problem for FGMs and the fully coupled partial slip contact problem for a graded layer. A linear multilayer model was developed by Ke and Wang [8] to analyze the fretting contact problem for FGM coating structures. Such studies in the fields of tribology and contact mechanics suggest that resistance to contact deformation and damage can be improved by using FGM coatings [9–18].

✉ L. L. Ke
llke@bjtu.edu.cn

[1] College of Engineering, Huazhong Agricultural University, Wuhan 430070, China

[2] Institute of Engineering Mechanics, Beijing Jiaotong University, Beijing 100044, China

In recent years, researchers have paid more attention to the thermoelastic contact of FGMs, due to their excellent thermomechanical properties. Since FGMs are frequently used in high-temperature environments, it is important to understand their thermoelastic contact properties for use in practical applications. It was Choi and Paulino [19] and Barik et al. [20] who first tried to investigate the thermoelastic contact problem of FGM coatings and interlayers, investigating the effect of frictional heat generation on the contact stress distributions. With consideration of frictional heat, Shahzamanian et al. [21,22] used the finite element method to solve the temperature and contact stress distributions in an FGM rotating brake disk. The thermoelastic frictional contact problem of a graded layer was investigated by Chen et al. [23,24], who also discussed the interface traction and temperature distribution under a prescribed thermoelastic environment for different parameter combinations. The cited results show that FGMs have great potential to provide better resistance in such thermoelastic contact problems.

For the sliding frictional contact problem, the frictional heat generation at the contact interface depends on the contact pressure, friction coefficient, and sliding speed. If the sliding speed exceeds a critical value, the contact becomes unstable under small perturbations. This class of instability involving coupled thermal and mechanical effects is called frictionally excited thermoelastic instability (TEI) [25]. The hot spot

and hot judder effects in brakes and clutches are related to TEI. Some numerical and theoretical results have shown that FGMs have potential to enhance the stability behavior of brake and clutch systems [26–29]. The frictionally excited TEI of FGMs in brake and clutch systems was first considered [26–28], including the thermoelastic contact problems of an FGM-coated disk, an FGM half-plane sliding against a homogeneous half-plane, and an FGM layer sliding against two homogeneous half-planes. It was observed by Hernik [29] that application of FGMs in brake disk structures can reduce the possibility of TEI, compared with homogeneous materials. These results showed that FGMs can delay interface separation and improve contact stability in frictional sliding systems.

Work by Afferrante et al. [30–34] revealed that the inherent elastodynamic vibration mode becomes unstable because of the extremely weak coupling between elastodynamic and thermoelastic effects, resulting in instability of the system at any, low speed. This new phenomenon is known as thermoelastic dynamic instability (TEDI). They considered a homogeneous elastic layer sliding against a rigid half-plane and two conducting elastic half-spaces sliding each other. More recently, Liu et al. [35] investigated the TEDI of an elastic half-plane sliding against a homogeneous layer half-plane. Because of the advantages of FGMs in improving frictionally excited TEI, we believe that FGMs could be further used to improve the TEDI of sliding systems. However, to date, literature on TEDI of FGMs remains very limited. The dynamic instability of an FGM-coated structure with exponentially varying elastic properties was analyzed recently by Liu et al. [36]. However, they did not consider the thermal effect on the dynamic contact characteristics of the FGM.

In the present study, we examined the stability of the thermoelastic wave caused by a perturbation in an FGM-coated structure, with consideration of frictional heat. The thermoelastic properties of the FGM coating are assumed to vary exponentially through the coating thickness. The effects of the gradient index, friction coefficient, and sliding speed on the TEDI of the sliding system are discussed. Furthermore, the transverse normal stress distribution in the depth direction is calculated for a homogeneous half-plane with an FGM or homogeneous coating.

We studied the TEI of FGMs in our previous papers [36–38]. However, that work considered the dynamic instability of the FGM coating structure without taking account of the thermal effect [36] or only studied the static thermoelastic instability of FGMs induced by the pressure-dependent thermal contact resistance [37, 38]. In this paper, we attempt to improve these studies by: (1) taking account of the coupling between thermal and dynamic effects, (2) considering the dynamic effect on the TEI of FGMs, and (3) paying special attention to the thermal stress distribution in FGM-coated structures, which is important for understanding interfacial failure.

2 Problem description

In this paper, we consider a homogeneous elastic, conducting half-plane (half-plane 2 in Fig. 1) sliding (with relative speed $\hat{V}_0$) against an FGM-coated half-plane (half-plane 1 in Fig. 1). As shown in Fig. 1, the normal force $\hat{P}_0$ and tangential force $\hat{Q}_0$ are applied to half-plane 2. Coulomb friction is assumed to occur at the contact surface, i.e.,

$$\hat{Q}_0 = f\hat{P}_0, \tag{1}$$

with f being the friction coefficient, generating heat at the interface. The heat flux is equal to the product of the contact pressure, friction coefficient, and sliding speed

$$q = f\hat{P}_0\hat{V}_0. \tag{2}$$

The contact problem is defined in a coordinate system $(\hat{x}, \hat{y})$ moving with constant speed $\hat{V}$, where $\hat{V}$ does not necessarily equal $\hat{V}_0$. The homogeneous half-plane 1 and half-plane 2 have mass density ρ_1 and ρ_2, shear modulus μ_1 and μ_2, thermal expansion coefficient α_1 and α_2, thermal conduction coefficient K_1 and K_2, and thermal diffusivity coefficient k_1 and k_2, respectively. It is assumed that the FGM coating and the lower half-plane are perfectly bonded to each other, and that the thermoelastic properties of the FGM vary in the thickness direction according to the exponential forms

$$\begin{aligned} &\rho(\hat{y}) = \rho_0 e^{\varepsilon\hat{y}},\ \mu(\hat{y}) = \mu_0 e^{\varepsilon\hat{y}},\ \alpha(\hat{y}) = \alpha_0 e^{\eta\hat{y}},\\ &K(\hat{y}) = K_0 e^{\tau\hat{y}}, \end{aligned} \tag{3}$$

where ρ_0, μ_0, α_0, and K_0 are the mass density, shear modulus, thermal expansion coefficient, and thermal conduction coefficient at the bottom ($\hat{y} = 0$) of the FGM coating, respectively, while ε, η, and τ are the gradient indexes. The Poisson's ratio and thermal diffusivity coefficient are assumed to be constant (ν_0 and k_0) for simplicity.

We now study the stability of the above sliding system. We assume that the system is disturbed by a small perturbation, then analyze the properties of the thermoelastic wave formed and propagating in it. The sliding is stable if this thermoelastic wave decays with time; otherwise, the sliding is unstable.

For linear isotropic elastic half-planes, the thermoelastic wave motion equations based on the moving coordinate system can be written as

$$\frac{\partial^2\hat{\theta}}{\partial\hat{x}^2} + \frac{\partial^2\hat{\theta}}{\partial\hat{y}^2} = \frac{1}{k}\left(\frac{\partial\hat{\theta}}{\partial\hat{t}} - \hat{V}\frac{\partial\hat{\theta}}{\partial\hat{x}}\right), \tag{4}$$

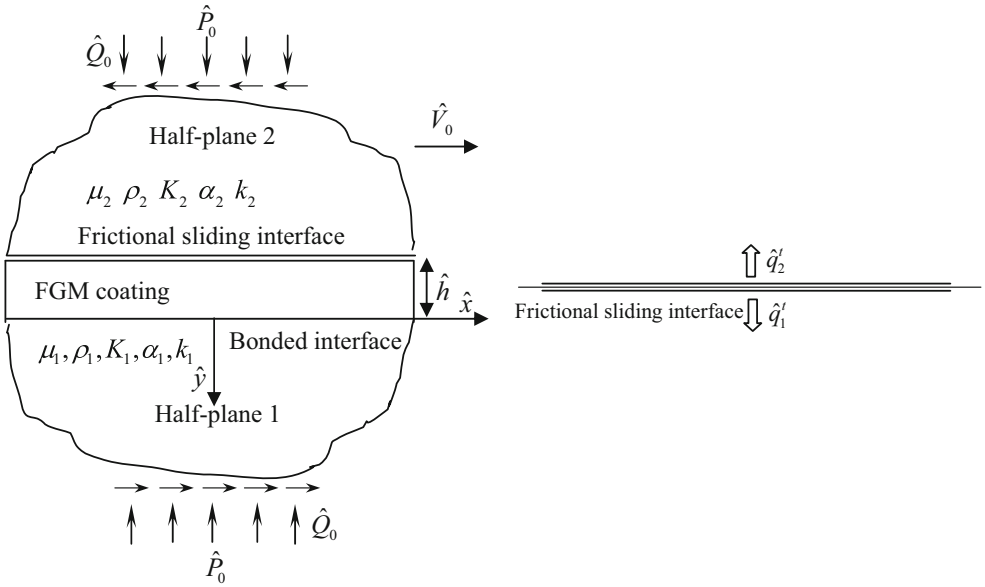

Fig. 1 Homogeneous elastic half-plane sliding against an FGM-coated half-plane

$$\frac{2(1-\nu)}{1-2\nu}\frac{\partial^2\hat{u}_x}{\partial\hat{x}^2}+\frac{\partial^2\hat{u}_x}{\partial\hat{y}^2}+\frac{1}{1-2\nu}\frac{\partial^2\hat{u}_y}{\partial\hat{y}\partial\hat{x}}-\frac{2(1+\nu)\alpha}{1-2\nu}\frac{\partial\hat{\theta}}{\partial\hat{x}}=\frac{\rho}{\mu}\left(\frac{\partial^2\hat{u}_x}{\partial\hat{t}^2}+\hat{V}^2\frac{\partial^2\hat{u}_x}{\partial\hat{x}^2}-2\hat{V}\frac{\partial^2\hat{u}_x}{\partial\hat{x}\partial\hat{t}}\right), \tag{5}$$

$$\frac{2(1-\nu)}{1-2\nu}\frac{\partial^2\hat{u}_y}{\partial\hat{y}^2}+\frac{\partial^2\hat{u}_y}{\partial\hat{x}^2}+\frac{1}{1-2\nu}\frac{\partial^2\hat{u}_x}{\partial\hat{y}\partial\hat{x}}-\frac{2(1+\nu)\alpha}{1-2\nu}\frac{\partial\hat{\theta}}{\partial\hat{y}}=\frac{\rho}{\mu}\left(\frac{\partial^2\hat{u}_y}{\partial\hat{t}^2}+\hat{V}^2\frac{\partial^2\hat{u}_y}{\partial\hat{x}^2}-2\hat{V}\frac{\partial^2\hat{u}_y}{\partial\hat{x}\partial\hat{t}}\right), \tag{6}$$

where ν is the Poisson's ratio. For the FGM coating, the thermoelastic wave motion equations are

$$\frac{\partial^2\hat{\theta}}{\partial\hat{x}^2}+\frac{\partial^2\hat{\theta}}{\partial\hat{y}^2}+\tau\frac{\partial\hat{\theta}}{\partial\hat{y}}=\frac{1}{k_0}\left(\frac{\partial\hat{\theta}}{\partial\hat{t}}-\hat{V}\frac{\partial\hat{\theta}}{\partial\hat{x}}\right), \tag{7}$$

$$\frac{2(1-\nu_0)}{1-2\nu_0}\frac{\partial^2\hat{u}_x}{\partial\hat{x}^2}+\frac{\partial^2\hat{u}_x}{\partial\hat{y}^2}+\frac{1}{1-2\nu_0}\frac{\partial^2\hat{u}_y}{\partial\hat{x}\partial\hat{y}}+\varepsilon\left(\frac{\partial\hat{u}_x}{\partial\hat{y}}+\frac{\partial\hat{u}_y}{\partial\hat{x}}\right)-\frac{2(1+\nu_0)}{1-2\nu_0}\alpha e^{\eta\hat{y}}\frac{\partial\hat{\theta}}{\partial\hat{x}}=\frac{\rho_0}{\mu_0}\left(\frac{\partial^2\hat{u}_x}{\partial\hat{t}^2}+\hat{V}^2\frac{\partial^2\hat{u}_x}{\partial x^2}-2\hat{V}\frac{\partial^2\hat{u}_x}{\partial\hat{x}\partial\hat{t}}\right), \tag{8}$$

$$\frac{2(1-\nu_0)}{1-2\nu_0}\frac{\partial^2\hat{u}_y}{\partial\hat{y}^2}+\frac{\partial^2\hat{u}_y}{\partial\hat{x}^2}+\frac{1}{1-2\nu_0}\frac{\partial^2\hat{u}_x}{\partial\hat{x}\partial\hat{y}}+\varepsilon\left[\frac{2(1-\nu_0)}{1-2\nu_0}\frac{\partial\hat{u}_y}{\partial\hat{y}}+\frac{2\nu_0}{1-2\nu_0}\frac{\partial\hat{u}_x}{\partial\hat{x}}\right]-\frac{2(1+\nu_0)}{1-2\nu_0}(\eta+\varepsilon)\alpha_0 e^{\eta\hat{y}}\hat{\theta}-\frac{2(1+\nu_0)}{1-2\nu_0}\alpha_0 e^{\eta\hat{y}}\frac{\partial\hat{\theta}}{\partial\hat{y}}=\frac{\rho_0}{\mu_0}\left(\frac{\partial^2\hat{u}_y}{\partial\hat{t}^2}+\hat{V}^2\frac{\partial^2\hat{u}_y}{\partial\hat{x}^2}-2\hat{V}\frac{\partial^2\hat{u}_y}{\partial\hat{x}\partial\hat{t}}\right). \tag{9}$$

In the next sections, we examine the stability of the thermoelastic wave by solving Eqs. (4)–(9) under the boundary conditions.

3 Thermoelastic wave field

The following quantities are introduced:

$$x=\hat{x}/l,\ y=\hat{y}/l,\ t=\hat{t}c_s/l,\ V=\hat{V}/\hat{V}c_sc_s,$$

$$c_s=\sqrt{\mu/\rho},\ \theta=\frac{\hat{\theta}\alpha(1+\nu)}{(1-\nu)}, \tag{10a}$$

$$u_x(x,y,t)=\hat{u}_x(\hat{x},\hat{y},\hat{t})/l,\ u_y(x,y,t)=\hat{u}_y(\hat{x},\hat{y},\hat{t})/l. \tag{10b}$$

These are made dimensionless using the characteristic length l defined as

$$l=\frac{\lambda}{2\pi}=\frac{1}{\omega}, \tag{11}$$

where ω and λ are the wavenumber and wavelength of the perturbation, respectively. Using the dimensionless quantities, the thermoelastic wave motion Eqs. (4)–(6) can be expressed in dimensionless form as

$$\frac{\partial^2\theta_j}{\partial x^2}+\frac{\partial^2\theta_j}{\partial y^2}=\frac{\hat{k}_j}{\gamma}\left(\frac{\partial\theta_j}{\partial t}-V_j\frac{\partial\theta_j}{\partial x}\right), \tag{12}$$

$$\beta_j^2\frac{\partial^2u_{xj}}{\partial x^2}+\frac{\partial^2u_{xj}}{\partial y^2}+\left(\beta_j^2-1\right)\frac{\partial^2u_{yj}}{\partial x\partial y}-\beta_j^2\frac{\partial\theta_j}{\partial x}=\chi_j^2\left(\frac{\partial^2u_{xj}}{\partial t^2}+V_j^2\frac{\partial^2u_{xj}}{\partial x^2}-2V_j\frac{\partial^2u_{xj}}{\partial x\partial t}\right), \tag{13}$$

$$\beta_j^2\frac{\partial^2 u_{yj}}{\partial y^2}+\frac{\partial^2 u_{yj}}{\partial x^2}+\left(\beta_j^2-1\right)\frac{\partial^2 u_{xj}}{\partial x\partial y}-\beta_j^2\frac{\partial\theta_j}{\partial y}$$
$$=\chi_j^2\left(\frac{\partial^2 u_{yj}}{\partial t^2}+V_j^2\frac{\partial^2 u_{yj}}{\partial x^2}-2V_j\frac{\partial^2 u_{yj}}{\partial x\partial t}\right), \tag{14}$$

where

$$\beta_j^2=2(1-\nu_j)/(1-2\nu_j),\quad k_j=k_1/k_j,\quad \chi_j=c_{sj}/c_{s1},$$
$$\gamma=k_1/(c_{s1}l),\quad V_j=\hat{V}_j/c_{s1}, \tag{15}$$

with subscripts $j=1,2$ denoting the half-planes 1 and 2, respectively, and $V_2-V_1=V_0$, $V_0=\hat{V}_0/\hat{V}_0c_{s1}$. It is assumed that the constant $\hat{V}_1$ and $\hat{V}_2$ are the sliding speeds of the half-planes 1 and 2, respectively.

For the FGM coating, Eqs. (7)–(9) can be rewritten as

$$\frac{\partial^2\theta_0}{\partial x^2}+\frac{\partial^2\theta_0}{\partial y^2}+\tau'\frac{\partial\theta_0}{\partial y}=\frac{\hat{k}}{\gamma}\left(\frac{\partial\theta_0}{\partial t}-V_1\frac{\partial\theta_0}{\partial x}\right), \tag{16}$$
$$\beta_0^2\frac{\partial^2 u_{x0}}{\partial x^2}+\frac{\partial^2 u_{x0}}{\partial y^2}+\left(\beta_0^2-1\right)\frac{\partial^2 u_{y0}}{\partial x\partial y}$$
$$+\varepsilon'\left(\frac{\partial u_{x0}}{\partial y}+\frac{\partial u_{y0}}{\partial x}\right)-\beta_0^2\mathrm{e}^{\eta' y}\frac{\partial\theta_0}{\partial x}$$
$$=\chi_0^2\left(\frac{\partial^2 u_{x0}}{\partial t^2}+V_1^2\frac{\partial^2 u_{x0}}{\partial x^2}-2V_1\frac{\partial^2 u_{x0}}{\partial x\partial t}\right), \tag{17}$$
$$\beta_0^2\frac{\partial^2 u_{y0}}{\partial y^2}+\frac{\partial^2 u_{y0}}{\partial x^2}+\left(\beta_0^2-1\right)\frac{\partial^2 u_{x0}}{\partial x\partial y}$$
$$+\varepsilon'\left[\beta_0^2\frac{\partial u_{y0}}{\partial y}+\left(\beta_0^2-2\right)\frac{\partial u_{y0}}{\partial x}\right]$$
$$-\beta_0^2(\eta'+\varepsilon')\mathrm{e}^{\eta' y}\theta_0-\beta_0^2\mathrm{e}^{\eta' y}\frac{\partial\theta_0}{\partial y}$$
$$=\chi_0^2\left(\frac{\partial^2 u_{y0}}{\partial t^2}+V_1^2\frac{\partial^2 u_{y0}}{\partial x^2}-2V_1\frac{\partial^2 u_{y0}}{\partial x\partial t}\right), \tag{18}$$

with

$$\hat{k}=k_1/k_0,\ \beta_0^2=2(1-\nu_0)/(1-2\nu_0),\ \chi_0=c_{s1}/c_{s0},$$
$$c_{s0}=\sqrt{\mu_0/\rho_0},\ \tau'=\tau l,\ \varepsilon'=\varepsilon l,\ \eta'=\eta l. \tag{19}$$

In addition, the constitutive relations between the dimensionless stress and displacement are defined by

$$\sigma_{xxj}=\hat{\sigma}_{xxj}/\mu_j=\beta_j^2\mathrm{e}^{\varepsilon' y}\frac{\partial u_{xj}}{\partial x}+\left(\beta_j^2-2\right)\mathrm{e}^{\varepsilon' y}\frac{\partial u_{yj}}{\partial y}$$
$$-\beta_j^2\mathrm{e}^{(\varepsilon'+\eta')y}\theta_j, \tag{20}$$
$$\sigma_{yyj}=\hat{\sigma}_{yyj}/\mu_j=\beta_j^2\mathrm{e}^{\varepsilon' y}\frac{\partial u_{yj}}{\partial y}+\left(\beta_j^2-2\right)\mathrm{e}^{\varepsilon' y}\frac{\partial u_{xj}}{\partial x}$$
$$-\beta_j^2\mathrm{e}^{(\varepsilon'+\eta')y}\theta_j, \tag{21}$$
$$\sigma_{xyj}=\hat{\sigma}_{xyj}/\mu_j=\mathrm{e}^{\varepsilon' y}\left(\frac{\partial u_{xj}}{\partial y}+\frac{\partial u_{yj}}{\partial x}\right),\quad j=0,1,2. \tag{22}$$

We can obtain the constitutive relations for the lower and upper homogeneous half-planes from Eqs. (20)–(22) by setting $\varepsilon'=\eta'=0$.

We suppose a perturbed temperature and displacements of the form

$$\theta_j(x,y,t)=\Theta_j(y)\mathrm{e}^{bt+\mathrm{i}x}, \tag{23}$$
$$u_{xj}(x,y,t)=U_{xj}(y)\mathrm{e}^{bt+\mathrm{i}x}, \tag{24}$$
$$u_{yj}(x,y,t)=U_{yj}(y)\mathrm{e}^{bt+\mathrm{i}x}, \tag{25}$$

where $j=0,1,2$, $\mathrm{i}=\sqrt{-1}$, $\Theta_j(y)$, $U_{xj}(y)$, and $U_{yj}(y)$ are complex functions, and $b=b^{\mathrm{R}}+\mathrm{i}b^{\mathrm{I}}$. Thus b^{R} is the real part of b and represents the exponential growth rate of the disturbance. Note that b^{R} is positive for unstable sliding, zero at the threshold of instability, and negative for stable sliding.

Substituting Eqs. (23)–(25) into Eqs. (12)–(14) yields

$$k_1\Theta_j''-\left[\gamma+k_j(b-\mathrm{i}V_j)\right]\Theta_j=0, \tag{26}$$
$$U_{xj}''-\left[\beta_j^2+\chi_j^2(b-\mathrm{i}V_j)^2\right]U_{xj}$$
$$+\mathrm{i}\left(\beta_j^2-1\right)U_{yj}'-\mathrm{i}\beta_j^2\Theta_j=0, \tag{27}$$
$$\beta_j^2U_{yj}''-\left[1+\chi_j^2(b-\mathrm{i}V_j)^2\right]U_{yj}$$
$$+\mathrm{i}\left(\beta_j^2-1\right)U_{xj}'-\beta_j^2\Theta_j'=0, \tag{28}$$

with $j=1,2$. The general solutions for the lower half-plane can be expressed as

$$\Theta_1(y)=d_1A_{13}\mathrm{e}^{s_{13}y}, \tag{29}$$
$$U_{x1}(y)=A_{11}\mathrm{e}^{s_{11}y}+A_{12}\mathrm{e}^{s_{12}y}+A_{13}\mathrm{e}^{s_{13}y}, \tag{30}$$
$$U_{y1}(y)=a_{11}A_{11}\mathrm{e}^{s_{11}y}+a_{12}A_{12}\mathrm{e}^{s_{12}y}+a_{13}A_{13}\mathrm{e}^{s_{13}y}, \tag{31}$$

with

$$s_{11}=\sqrt{1+(b-\mathrm{i}V_1)^2},\quad s_{12}=\sqrt{1+(b-\mathrm{i}V_1)^2/\beta_1^2},$$
$$s_{13}=\sqrt{1+(b-\mathrm{i}V_1)/\gamma}, \tag{32}$$
$$a_{11}=1/(\mathrm{i}s_{11}),\ a_{12}=-\mathrm{i}s_{12},\ a_{13}=-\mathrm{i}s_{13},$$
$$d_1=(b-\mathrm{i}V_1)[\beta_1^2/\gamma-(b-\mathrm{i}V_1)]/(\mathrm{i}\beta_1^2). \tag{33}$$

and

$$\mathrm{Re}\{s_{11}\}<0,\quad \mathrm{Re}\{s_{12}\}<0,\quad \mathrm{Re}\{s_{13}\}<0. \tag{34}$$

The general solutions for the upper half-plane are

$$\Theta_2(y)=d_2A_{23}\mathrm{e}^{s_{23}y}, \tag{35}$$

$$U_{x2}(y) = A_{21}\mathrm{e}^{s_{21}y} + A_{22}\mathrm{e}^{s_{22}y} + A_{23}\mathrm{e}^{s_{23}y}, \tag{36}$$

$$U_{y2}(y) = a_{21}A_{21}\mathrm{e}^{s_{21}y} + a_{22}A_{22}\mathrm{e}^{s_{22}y} + a_{23}A_{23}\mathrm{e}^{s_{23}y}, \tag{37}$$

with

$$s_{21} = -\sqrt{1+\chi_2^2(b-\mathrm{i}V_2)^2}, \quad s_{22} = -\sqrt{1+\chi_2^2(b-\mathrm{i}V_2)^2/\beta_2^2},$$
$$s_{23} = -\sqrt{1+k_{21}(b-\mathrm{i}V_2)/\gamma}, \tag{38}$$
$$a_{21} = 1\big/(\mathrm{i}s_{21}),\ a_{22} = -\mathrm{i}s_{22},\ a_{23} = -\mathrm{i}s_{23},$$
$$d_2 = (b-\mathrm{i}V_2)\big[\beta_2^2 k_{21}\big/\gamma - \chi_2^2(b-\mathrm{i}V_2)\big]\big/(\mathrm{i}\beta_2^2), \tag{39}$$

and

$$\mathrm{Re}\{s_{21}\} > 0,\ \mathrm{Re}\{s_{22}\} > 0,\ \mathrm{Re}\{s_{23}\} > 0. \tag{40}$$

The general solutions for the FGM coating are given by

$$\Theta_0(y) = d_{05}A_{05}\mathrm{e}^{s_{05}y} + d_{06}A_{06}\mathrm{e}^{s_{06}y}, \tag{41}$$

$$U_{x0}(y) = \sum_{k=1}^{4} A_{0k}\mathrm{e}^{s_{0k}y} + A_{05}\mathrm{e}^{(s_{05}+\eta')y} + A_{06}\mathrm{e}^{(s_{06}+\eta')y}, \tag{42}$$

$$U_{y0}(y) = \sum_{k=1}^{4} a_{0k}A_{0k}\mathrm{e}^{s_{0k}y} + a_{05}A_{05}\mathrm{e}^{(s_{05}+\eta')y} + a_{06}A_{06}\mathrm{e}^{(s_{06}+\eta')y}, \tag{43}$$

where

$$s_{01} = -\frac{1}{2}\varepsilon' - \frac{1}{2\beta_0}\sqrt{q_1+q_2}, \quad s_{02} = -\frac{1}{2}\varepsilon' - \frac{1}{2\beta_0}\sqrt{q_1-q_2}, \tag{44a}$$

$$s_{03} = -\frac{1}{2}\varepsilon' + \frac{1}{2\beta_0}\sqrt{q_1+q_2}, \quad s_{04} = -\frac{1}{2}\varepsilon' + \frac{1}{2\beta_0}\sqrt{q_1-q_2}, \tag{44b}$$

$$s_{05} = -\tau'/2 + \sqrt{\tau'^2/4 + 1 + \hat{k}(b-\mathrm{i}V_1)/\gamma},$$
$$s_{06} = -\tau'/2 - \sqrt{\tau'^2/4 + 1 + \hat{k}(b-\mathrm{i}V_1)/\gamma}, \tag{44c}$$

with

$$q_1 = 2\chi_0^2(b-\mathrm{i}V_1)^2\left(\beta_0^2+1\right) + \beta_0^2\left(4+\varepsilon'^2\right),$$
$$q_2 = 2\sqrt{\chi_0^4(b-\mathrm{i}V_1)^4\left(\beta_0^2-1\right)^2 - 4\varepsilon'^2\beta_0^2\left(\beta_0^2-2\right)}, \tag{45}$$

and

$$a_{01} = \mathrm{i}\{-(\beta_0^2-1)[\chi_0^2(b-\mathrm{i}V_1)^2 + 2\beta_0^2] + q_2/2\}$$
$$/\{2\beta_0^2[\varepsilon' + (\beta_0^2-1)s_{01}]\}, \tag{46a}$$

$$a_{02} = -\mathrm{i}\big[2\varepsilon'\left(\beta_0^2-2\right) + 2s_{02}\left(\beta_0^2-1\right)\big]$$
$$/\big\{\left(\beta_0^2-1\right)\big[\chi_0^2(b-\mathrm{i}V_1)^2+2\big] - q_2/2\big\}, \tag{46b}$$

$$a_{03} = \mathrm{i}\big\{-\left(\beta_0^2-1\right)\big[\chi_0^2(b-\mathrm{i}V_1)^2 + 2\beta_0^2\big] + q_2/2\big\}$$
$$/\big\{2\beta_0^2\big[\varepsilon' + /\left(\beta_0^2-1\right)s_{03}\big]\big\}, \tag{46c}$$

$$a_{04} = -\mathrm{i}\big[2\varepsilon'\left(\beta_0^2-2\right) + 2s_{04}\left(\beta_0^2-1\right)\big]$$
$$/\big\{\left(\beta_0^2-1\right)\big[\chi_0^2(b-\mathrm{i}V_1)^2+2\big] - q_2/2\big\}, \tag{46d}$$

$$a_{0j} = \mathrm{i}\{[\hat{k}(b-\mathrm{i}V_1)/\gamma - \chi_0^2(b-\mathrm{i}V_1)^2$$
$$+ 3\eta'(\eta'-\tau') + (\tau'-\varepsilon')^2 + 4\varepsilon'\eta']s_{0j}$$
$$+ (3\eta' - \tau' + 2\varepsilon')\hat{k}(b-\mathrm{i}V_1)/\gamma - (\eta'+\varepsilon')\chi_0^2$$
$$(b-\mathrm{i}V_1)^2 + \eta'[(\eta'+\varepsilon')^2 + 2] - \tau'\}$$
$$/[\chi_0^2(b-\mathrm{i}V_1)^2 - \hat{k}(b-\mathrm{i}V_1)/\gamma - (2\eta'-\tau')s_{0j}$$
$$- \eta'^2 + \varepsilon'^2], \quad j = 5, 6, \tag{46e}$$

$$d_{0j} = -i\{(\varepsilon' + 2\eta' - \tau')\chi_0^2(b-i\,V_1)^2 s_{0j} + \beta_0^2(\varepsilon' + 2\eta' - \tau')$$
$$[-2\hat{k}(b-i\,V_1)/\gamma + \chi_0^2(b-i\,V_1)^2 + \varepsilon'(\tau'-2\eta')$$
$$- (\tau'-\eta')^2 - \eta'^2]s_{0j} - \beta_0^2[\hat{k}(b-i\,V_1)/\gamma]^2$$
$$2\varepsilon'^2 - \chi_0^4(b-i\,V_1)^4 - \beta_0^2[\hat{k}(b-i\,V_1)/\gamma]$$
$$[(2\eta'-\tau')^2 + 2\varepsilon'(3\eta'-\tau')\varepsilon'^2 + 2\eta'^2]$$
$$+ (1+\beta_0^2)[\hat{k}(b-i\,V_1)/\gamma + \eta'^2 + \varepsilon'\eta']$$
$$\chi_0^2(b-i\,V_1)^2\beta_0^2[(2\eta'-\tau')^2 + 2\varepsilon'(\eta'^3 - \tau' + 2\eta')$$
$$+ \varepsilon'^2(2+\eta'^2) + \eta'^4]\}$$
$$/\{\beta_0^2[\chi_0^2(b-i\,V_1)^2 - \hat{k}(b-i\,V_1)/\gamma$$
$$+ (\tau'-2\eta')s_{0j} - \eta'^5 + \varepsilon'^2]\}, \quad j = 5, 6. \tag{46f}$$

In Eqs. (32), (38), and (44), the multivalued "$\sqrt{\ }$" functions are taken as the branches with positive real part.

Since the FGM coating is perfectly bonded to half-plane 1, the components of the displacement and stress on the bonded interface ($y = 0$) satisfy the continuity conditions. We can write them in dimensionless form as

$$u_{x1}(x,0,t) = u_{x0}(x,0,t),\ u_{y1}(x,0,t) = u_{y0}(x,0,t), \tag{47}$$

$$\left(\mu_1\big/\mu_0\right)\sigma_{xy1}(x,0,t) = \sigma_{xy0}(x,0,t),$$
$$\left(\mu_1\big/\mu_0\right)\sigma_{yy1}(x,0,t) = \sigma_{yy0}(x,0,t). \tag{48}$$

The perturbation of temperature is also continuous at $y = 0$ as

$$\theta_1(x,0,t) = \frac{\theta_0(x,0,t)D_0\alpha_1}{\alpha_0},$$
$$\frac{K_1}{K_0}\left.\frac{\partial\theta_1(x,0,t)}{\partial y}\right|_{y=0} = \frac{\alpha_1 D_0}{\alpha_0}\left.\frac{\partial\theta_0(x,0,t)}{\partial y}\right|_{y=0}, \tag{49}$$

where

$$D_0 = \frac{\beta_0^2\left(3\beta_1^2-4\right)}{\beta_1^2\left(3\beta_0^2-4\right)}. \tag{50}$$

We can express Eqs. (47)–(49) in matrix form with the help of general solutions Eqs. (29)–(31) and Eqs. (41)–(43):

$$\boldsymbol{M}_1\left[\begin{array}{cccc} A_{11} & A_{12} & A_{13} \end{array}\right]^{\mathrm{T}} = \boldsymbol{M}_0\left[\begin{array}{cccccc} A_{01} & A_{02} & A_{03} & A_{04} & A_{05} & A_{06} \end{array}\right]^{\mathrm{T}}, \tag{51}$$

with

$$\boldsymbol{M}_1 = \left[\begin{array}{cccc} 1 & a_{11} & (s_{11}+\mathrm{i}a_{11})\mu_1/\mu_0 & \left[\beta_1^2 s_{11}a_{11}+\mathrm{i}\left(\beta_1^2-2\right)\right]\mu_1/\mu_0 \quad 0 \quad 0 \\ 1 & a_{12} & (s_{12}+\mathrm{i}a_{12})\mu_1/\mu_0 & \left[\beta_1^2 s_{12}a_{12}+\mathrm{i}\left(\beta_1^2-2\right)\right]\mu_1/\mu_0 \quad 0 \quad 0 \\ 1 & a_{13} & (s_{13}+\mathrm{i}a_{13})\mu_1/\mu_0 & \left[\beta_1^2 s_{13}a_{13}+\mathrm{i}\left(\beta_1^2-2\right)-\beta_1^2 d_{13}\right]\mu_1/\mu_0 \quad d_{13} \quad s_{13}d_{13}K_1/K_0 \end{array}\right]^{\mathrm{T}}, \tag{52a}$$

$$\boldsymbol{M}_0 = \left[\begin{array}{cccccc} 1 & a_{01} & s_{01}+\mathrm{i}a_{01} & \beta_0^2 s_{01}a_{01}+\mathrm{i}\left(\beta_0^2-2\right) & 0 & 0 \\ 1 & a_{02} & s_{02}+\mathrm{i}a_{02} & \beta_0^2 s_{02}a_{02}+\mathrm{i}\left(\beta_0^2-2\right) & 0 & 0 \\ 1 & a_{03} & s_{03}+\mathrm{i}a_{03} & \beta_0^2 s_{03}a_{03}+\mathrm{i}\left(\beta_0^2-2\right) & 0 & 0 \\ 1 & a_{04} & s_{04}+\mathrm{i}a_{04} & \beta_0^2 s_{04}a_{04}+\mathrm{i}\left(\beta_0^2-2\right) & 0 & 0 \\ 1 & a_{05} & s_{05}+\eta'+\mathrm{i}a_{05} & \beta_0^2\left(s_{05}+\eta'\right)a_{05}+\mathrm{i}\left(\beta_0^2-2\right)-\beta_0^2 d_{05} & D_0 d_{05}\alpha_1/\alpha_0 & D_0 s_{05}\alpha_1/\alpha_0 \\ 1 & a_{06} & s_{06}+\eta'+\mathrm{i}a_{06} & \beta_0^2\left(s_{06}+\eta'\right)a_{06}+\mathrm{i}\left(\beta_0^2-2\right)-\beta_0^2 d_{06} & D_0 d_{06}\alpha_1/\alpha_0 & D_0 s_{06}\alpha_1/\alpha_0 \end{array}\right]^{\mathrm{T}}. \tag{52b}$$

The solution of Eq. (51) is

$$A_{0k} = F_{k1}A_{11} + F_{k2}A_{12} + F_{k3}A_{13}, \quad k = 1, 2, \ldots, 6, \tag{53}$$

where F_{kj} is the element of matrix $\boldsymbol{M}_0^{-1}\boldsymbol{M}_1$. Finally, the dimensionless displacement and stress at the frictional sliding interface (with $y = -h$) are required to satisfy the boundary conditions

$$\begin{aligned} &\sigma_{xy0}(x,-h,t) = -f\sigma_{yy0}(x,-h,t), \\ &\sigma_{xy2}(x,-h,t) = -f\sigma_{yy2}(x,-h,t), \end{aligned} \tag{54}$$

$$\begin{aligned} &u_{y0}(x,-h,t) = u_{y2}(x,-h,t), \\ &\left(\mu_0/\mu_2\right)\sigma_{yy0}(x,-h,t) = \sigma_{yy2}(x,-h,t). \end{aligned} \tag{55}$$

Substituting Eqs. (35)–(37), Eqs. (41)–(43), and Eq. (53) into Eqs. (54) and (55) yields

$$A_{13} = \eta_{11}A_{11} + \eta_{12}A_{12}, \quad A_{23} = \eta_{21}A_{11} + \eta_{22}A_{12}, \tag{56}$$

$$A_{21} = l_{11}A_{11} + l_{12}A_{12}, \quad A_{22} = l_{21}A_{11} + l_{22}A_{12}, \tag{57}$$

where $\eta_{1j}, \eta_{2j}, l_{1j}$, and l_{2j} $(j = 1, 2)$ are given in the Appendix.

Half-plane 1 is regarded as stationary, while half-plane 2 moves along the x-direction with speed $\hat{V}_0$. Therefore, the dimensionless speed (V_s) and contact traction (P) at the contact interface are

$$P(x,0,t) = P_0 - \sigma_{yy0}\left(\mu_0/\mu_1\right), \tag{58}$$

$$V_\mathrm{s}(x,0,t) = V_0 - \left(\frac{\partial u_{x0}}{\partial t} - \frac{\partial u_{x2}}{\partial t}\right), \tag{59}$$

with $V_\mathrm{s}(x,0,t) = \hat{V}_\mathrm{s}(x,0,t)/C_{\mathrm{s}1}$ and $P_0 = \hat{P}_0/\mu_1$. In addition, we consider that the frictional heat, the continuity of temperature, and the heat flux on the frictional sliding interface $(y = -h)$ can be formulated as

$$\theta_0(x,h,t) = D_2\alpha_0\theta_2(x,h,t)/\alpha_2, \tag{60}$$

$$\begin{aligned} &\hat{q}_2(x,h,t) + \hat{q}_0(x,h,t) \\ &\quad = fP(x,h,t)V_\mathrm{s}(x,h,t) - fP_0V_0, \end{aligned} \tag{61}$$

with

$$D_2 = \frac{\beta_2^2\left(3\beta_0^2-4\right)}{\beta_0^2\left(3\beta_2^2-4\right)}. \tag{62}$$

Substituting Eqs. (58) and (59) into Eq. (61) and dropping the second-order term in the product (PV_s) yields

$$\begin{aligned} &-\frac{\alpha_0/\alpha_2}{K_0/K_2}D_2\frac{\partial\theta_2(x,h,t)}{\partial y} + \mathrm{e}^{\tau' h}\frac{\partial\theta_0(x,h,t)}{\partial y} \\ &\quad = \frac{fH_1}{2\gamma}\xi\left[\left(\frac{\partial u_{x2}(x,h,t)}{\partial t} - \frac{\partial u_{x0}(x,h,t)}{\partial t}\right)P_0 - \frac{\mu_0 V_0\sigma_{yy0}(x,h,t)}{\mu_1}\right], \end{aligned} \tag{63}$$

with

$$H_1 = \frac{2\mu_1\alpha_1 k_1}{K_1}\frac{1+\nu_1}{1-\nu_1}, \quad \xi = \frac{K_1/K_0}{\alpha_1/\alpha_0}\frac{1}{D_0}. \tag{64}$$

Substitution Eqs. (35)–(37), Eqs. (41)–(43), and Eqs. (58) and (59) into Eqs. (60) and (63) yields

$$g_{11}A_{11} + g_{12}A_{12} = 0, \quad g_{21}A_{11} + g_{22}A_{12} = 0, \tag{65}$$

with

$$
\begin{aligned}
g_{1j} &= \left(d_{05}F_{53}\mathrm{e}^{s_{05}h} + d_{06}F_{63}\mathrm{e}^{s_{06}h}\right)\eta_{1j} \\
&\quad - D_2 d_{23}\mathrm{e}^{s_{23}h}(\eta_{21}l_{1j} + \eta_{22}l_{2j})\alpha_0/\alpha_2, \qquad (66)\\
g_{2j} &= \frac{fH_1}{2\gamma}\xi\sum_{k=1}^{4}\left(P_0 b + V_0\mathrm{e}^{\varepsilon' h}\gamma_{2k}^{F}\mu_0/\mu_1\right) \\
&\quad (F_{kj} + \eta_{1j}F_{k3})\mathrm{e}^{s_{0k}h} \\
&\quad + \frac{fH_1}{2\gamma}\xi\sum_{k=5}^{6}\{V_0\mathrm{e}^{\varepsilon' h}[\beta_0^2 a_{0k}(s_{0k}+\eta') + \mathrm{i}(\beta_0^2 - 2)] \\
&\quad \mu_0/\mu_1 + P_0 b\}F_{k3}\mathrm{e}^{(s_{0k}+\eta')h}\eta_{1j} \\
&\quad - \frac{fH_1}{2\gamma}\xi V_0\beta_0^2\mathrm{e}^{(\varepsilon'+\eta')h}\left(d_{05}F_{53}\mathrm{e}^{s_{05}h} + d_{06}F_{63}\mathrm{e}^{s_{06}h}\right) \\
&\quad \eta_{1j}\mu_0/\mu_1 \\
&\quad + \mathrm{e}^{\tau' h}\left(d_{05}s_{05}F_{53}\mathrm{e}^{s_{05}h} + d_{06}s_{06}F_{63}\mathrm{e}^{s_{06}h}\right)\eta_{1j} \\
&\quad - \frac{fH_1}{2\gamma}\xi P_0 b\left(l_{1j}\mathrm{e}^{s_{21}h} + l_{2j}\mathrm{e}^{s_{22}h}\right) \\
&\quad - \left(\frac{fH_1}{2\gamma}\xi P_0 b + \frac{\alpha_0/\alpha_2}{K_0/K_2}D_2 d_{23}s_{23}\right) \\
&\quad (\eta_{21}l_{1j} + \eta_{22}l_{2j})\mathrm{e}^{s_{23}h}, \quad j = 1, 2. \qquad (67)
\end{aligned}
$$

The nontrivial solution of Eq. (65) requires

$$g_{11}g_{22} - g_{12}g_{21} = 0. \qquad (68)$$

When the material properties, friction coefficient, and sliding speed are given, the complex nonlinear Eq. (68) can be solved using the iterative method and the unknown complex b obtained. Then, at the contact interface, the dimensionless contact traction (P) and dimensionless speed (V_s) can be calculated via

$$
\begin{aligned}
P(x, -h, t) &= P_0 - (\mu_0/\mu_1)C_1 A_{11}\mathrm{e}^{bt+\mathrm{i}x}, \\
V_s(x, -h, t) &= V_0 - bC_2 A_{11}\mathrm{e}^{bt+\mathrm{i}x}, \qquad (69)
\end{aligned}
$$

with

$$
\begin{aligned}
C_1 &= \mathrm{e}^{\varepsilon' h}\sum_{k=1}^{4}\gamma_{2k}\left[F_{k1} - F_{k2}g_{12}/g_{11}\right. \\
&\quad \left. + F_{k3}\left(\eta_{11} - \eta_{12}g_{11}/g_{12}\right)\right]\mathrm{e}^{s_{0k}h} \\
&\quad + \mathrm{e}^{\varepsilon' h}\sum_{k=5}^{6}\left[\beta_0^2\left(s_{0k}+\eta'\right)a_{0k} + \mathrm{i}\left(\beta_0^2 - 2\right)\right] \\
&\quad F_{k3}\left(\eta_{11} - \eta_{12}g_{11}/g_{12}\right)\mathrm{e}^{(s_{0k}+\eta')h} \\
&\quad - \beta_0^2\mathrm{e}^{(\varepsilon'+\eta')h}\left(d_{05}F_{53}\mathrm{e}^{s_{05}h} + d_{06}F_{63}\mathrm{e}^{s_{06}h}\right) \\
&\quad \left(\eta_{11} - \eta_{12}g_{11}/g_{12}\right), \qquad (70)
\end{aligned}
$$

$$
\begin{aligned}
C_2 &= \sum_{k=1}^{4}\left(F_{k1} - F_{k2}g_{11}/g_{12}\right)\mathrm{e}^{s_{0k}h} \\
&\quad + \left[F_{53}\mathrm{e}^{(s_{05}+\eta')h} + F_{63}\mathrm{e}^{(s_{06}+\eta')h}\right] \\
&\quad \times \left(\eta_{11} - \eta_{12}g_{11}/g_{12}\right) \\
&\quad - \left[\left(\mathrm{e}^{s_{21}h} + \eta_{21}\mathrm{e}^{s_{23}h}\right)\left(l_{11} - l_{12}g_{11}/g_{12}\right)\right. \\
&\quad + \left(\mathrm{e}^{s_{22}h} + \eta_{22}\mathrm{e}^{s_{23}h}\right) \\
&\quad \left. \times \left(l_{21} - l_{22}g_{11}/g_{12}\right)\right]. \qquad (71)
\end{aligned}
$$

4 Results and discussion

When the effect of the material gradient property is neglected, we can simplify the problem as two half-planes sliding against each other, just like the study of the TEDI by Afferrante et al. [34] between two frictional sliding elastic homogeneous half-spaces. Thus we conduct a direct comparison between those results reported by Afferrante et al. [34] and ours. The effect of the sliding speed (V_0) on the critical friction efficient (f_{cr}) is presented in Fig. 2, revealing excellent agreement between the present results and those in Ref. [34].

The dynamic instability of the FGM-coated structure was analyzed by Liu et al. [36], who found that the instability of the Adams' family wave occurs at almost zero friction with small mass density ratio ρ_2/ρ_1. For the Rice's family wave, the instability occurs at small friction when the mass density ratio ρ_2/ρ_1 is more 10 times larger than the modulus ratio μ_2/μ_1. However, the material combination in the latter case is rare in nature. Furthermore, the thermoelastic dynamic instability of the homogeneous coated structure was studied by Liu et al. [35], who found that the Adams' family wave was more susceptible to thermoelastic dynamic instability than the Rice's family wave for the same material combinations.

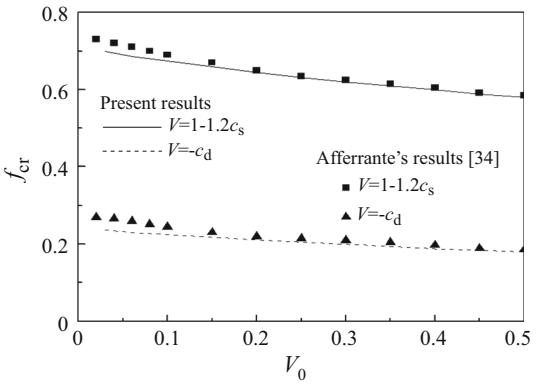

Fig. 2 Relations of f_{cr} versus V_0 for $P_0 = 0.1$, $\chi = 0.2$, $\gamma = 10^{-4}$, $\alpha_1/\alpha_2 = 1.2$, $k_1/k_2 = 0.1$, and $K_1/K_2 = 0.1$

Therefore, this paper only presents the stability of Adams' family wave for common material combinations and small friction coefficient. We assume that the reference coordinate system is fixed to the lower FGM-coated half-plane, i.e., $V_1 = 0$ and $V_2 = -V_0$. The thermoelastic properties are continuous at the bonded interface $y = 0$, i.e., $\rho_0 = \rho_1$, $\mu_0 = \mu_1$, $\alpha_0 = \alpha_1$, $K_1 = K_2$, and $k_0 = k_1$, and the gradient indexes satisfy $\varepsilon' = \tau' = \eta' = \lambda$. Also, the Poisson's ratios of all materials are chosen as $\nu_1 = \nu_0 = \nu_2 = 0.25$, $\gamma = 10^{-4}$, and $H_1 = 1$ [30,39].

4.1 Effect of gradient index on TEDI

Figures 3, 4, and 5 show the relations of the dimensionless gradient index (λ) and exponential growth rate b^{R} for various material combinations (χ_2^2, μ_1/μ_2). It is seen that b^{R} remains unchanged when λ is less than a certain negative value; if λ is further increased, b^{R} fluctuates and then decreases gradually to zero. For given shear wave speed ratio (χ_2^2), b^{R} increases with decrease of μ_1/μ_2 when λ is positive and $\chi_2^2 \leq 1$; b^{R} increases with increase of μ_1/μ_2, and the range of λ for instability increases when $\chi_2^2 > 1$ (Fig. 3). For given shear modulus ratio μ_1/μ_2, b^{R} increases with decrease of χ_2^2. The range of λ for instability increases when λ is larger than a certain positive value (Fig. 4). Figure 5 shows that b^{R} decreases with increase of μ_1/μ_2 when we select $\chi_2^2 = \mu_1/\mu_2$. Interestingly, one can observe that the sliding is stable when the gradient index is larger than a certain positive value, remains unchanged when the gradient index is less than a certain negative value, and fluctuates with change of the gradient index from negative to positive.

4.2 Effects of friction coefficient and sliding speed on TEDI

Figure 6 shows the relations of the friction coefficient f and exponential growth rate b^{R} for different values of the gradient index λ. Note that, for fixed gradient index λ, b^{R} increases with increase of the friction coefficient. It is also seen that different values of the gradient index correspond to different critical friction coefficients. The relations of the dimensionless sliding speed V_0 and exponential growth rate b^{R} for some selected values of gradient index λ are presented in Fig. 7. Note that b^{R} decreases gradually to zero with increase of the sliding speed. This implies that the system is susceptible to TEDI even at small sliding speed. We define a critical sliding speed V_{cr} when the exponential growth rate b^{R} is zero. It is also shown that, for fixed V_0, this critical sliding speed V_{cr} increases with increase of the gradient index. These results imply that one can modify the sliding stability, critical friction coefficient, and critical sliding speed by adjusting the gradient index of the FGM coating.

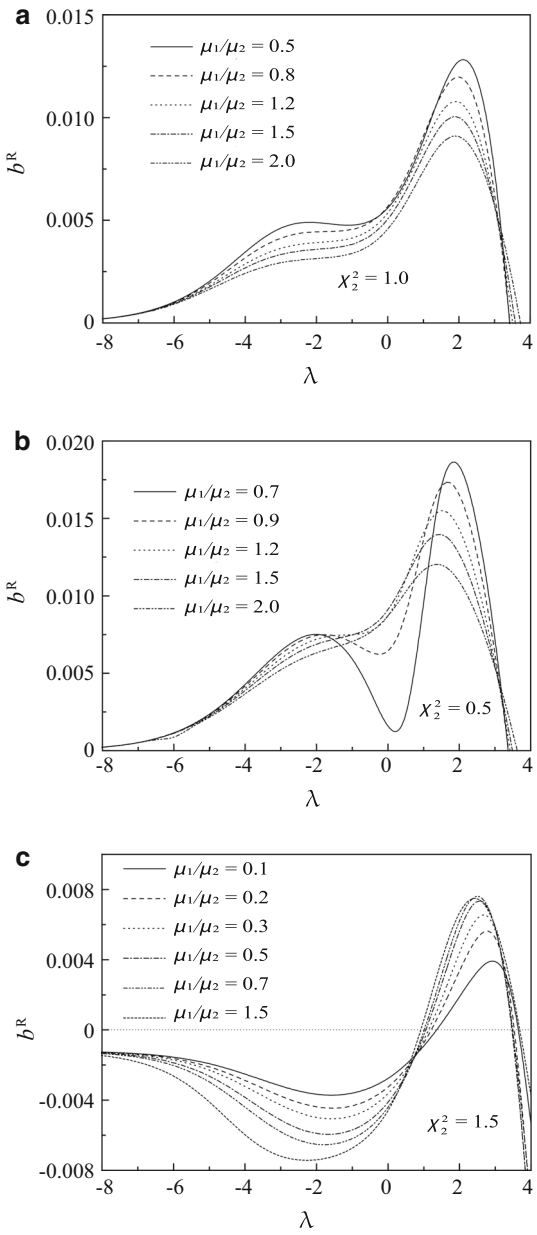

Fig. 3 Relations of b^{R} versus λ with $k_1/k_2 = 0.1$, $\alpha_1/\alpha_2 = 1.2$, and $K_1/K_2 = 0.1$: **a** χ_2^2=1.0, **b** χ_2^2=0.5, **c** χ_2^2=1.5

4.3 Thermal stress distribution

It is known that FGM coatings are better for controlling interfacial tensile stress compared with homogeneous coatings. This can improve sliding stability and reduce the possibility of interfacial failure [36]. To confirm this advantage of FGM coatings, this section presents the distribution of transverse normal thermal stress in the thickness direction, and examines the effect of the FGM coating on it. We discuss two cases: (1) an FGM coating with continuous material properties at the bonded interface $y = 0$, i.e., $\rho_0 = \rho_1$, μ_0

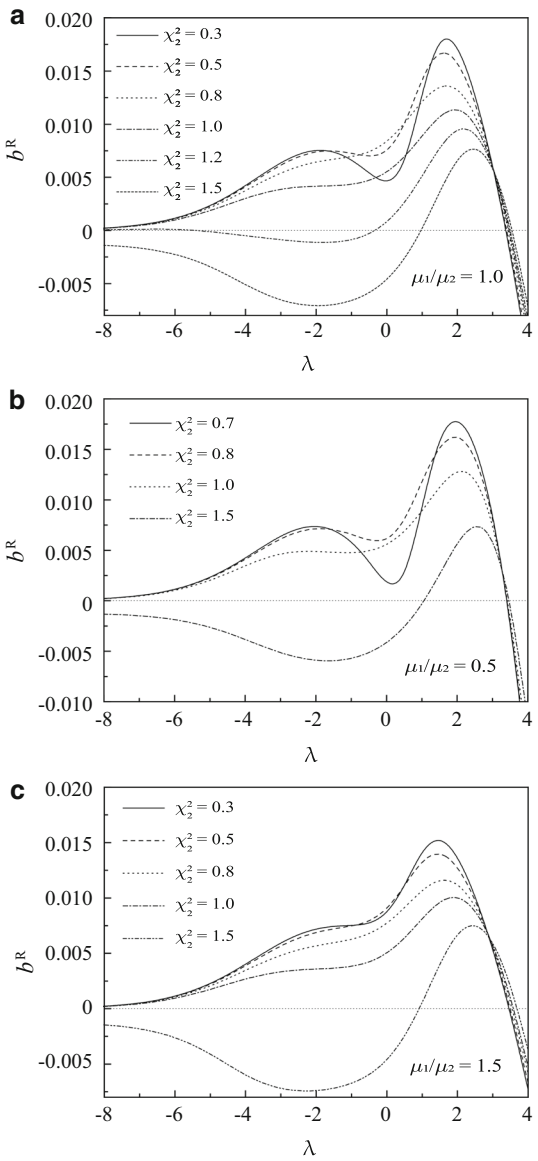

Fig. 4 Relations of b^R versus λ with $k_1/k_2 = 0.1$, $\alpha_1/\alpha_2 = 1.2$, and $K_1/K_2 = 0.1$: **a** μ_1/μ_2=1.0, **b** μ_1/μ_2= 0.5, **c** μ_1/μ_2=1.5

$= \mu_1$, $\alpha_0 = \alpha_1$, $K_0 = K_1$, and $k_0 = k_1$, where the material parameters of the lower and upper half-planes satisfy $\mu_1/\mu_2 = \alpha_1/\alpha_2 = k_1/k_2 = K_1/K_2 = \psi$, and the coating gradient index is defined as $\lambda = \ln(1/\psi)/(-h)$; (2) a homogeneous coating with the same material properties as those of the upper half-plane.

As the stress increases with time, the calculation is for the moment when loss of contact is just initiated, i.e.,

$$P_0 = \left|(\mu_0/\mu_1)C_1A_{11}e^{b^R t}\right|, \tag{72}$$

with

$$|A_{11}| = P_0/|(\mu_0/\mu_1)C_1e^{b^R t}|. \tag{73}$$

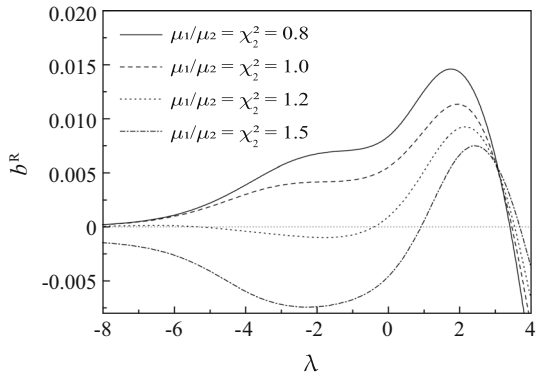

Fig. 5 Relations of b^R versus λ with $k_1/k_2 = 0.1$, $\alpha_1/\alpha_2 = 1.2$, and $K_1/K_2 = 0.1$

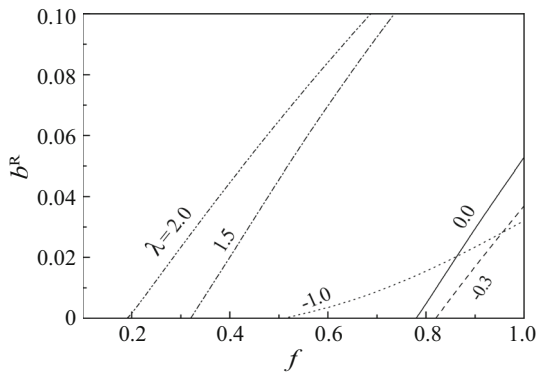

Fig. 6 Relations of b^R versus f with $P_0 = 0.1$, $V_0 = 0.1$, $\chi_2^2 = 0.3$, μ_1/μ_2= 0.3, $k_1/k_2 = 0.1$, $\alpha_1/\alpha_2 = 1.2$, and $K_1/K_2 = 0.1$

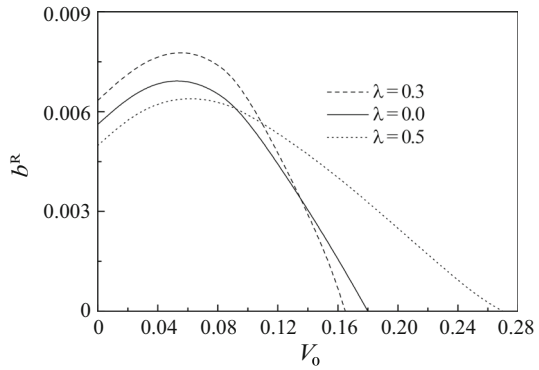

Fig. 7 Relations of b^R versus V_0 with $f = 0.2$, $P_0 = 0.1$, $\chi_2^2 = 0.8$, μ_1/μ_2= 0.5, $k_1/k_2 = 0.1$, $\alpha_1/\alpha_2 = 1.2$, and $K_1/K_2 = 0.1$

Then, for the FGM-coated structure, the amplitude of the tensile stresses can be expressed as

$$|\sigma_{xx0}| = P_0\left|E_0/\left(C_1\mu_0/\mu_1\right)\right|, \tag{74a}$$

$$|\sigma_{xx1}| = P_0\left|E_1/\left(C_1\mu_0/\mu_1\right)\right|, \tag{74b}$$

$$|\sigma_{xx2}| = P_0\left|E_2/\left(C_1\mu_0/\mu_1\right)\right|, \tag{74c}$$

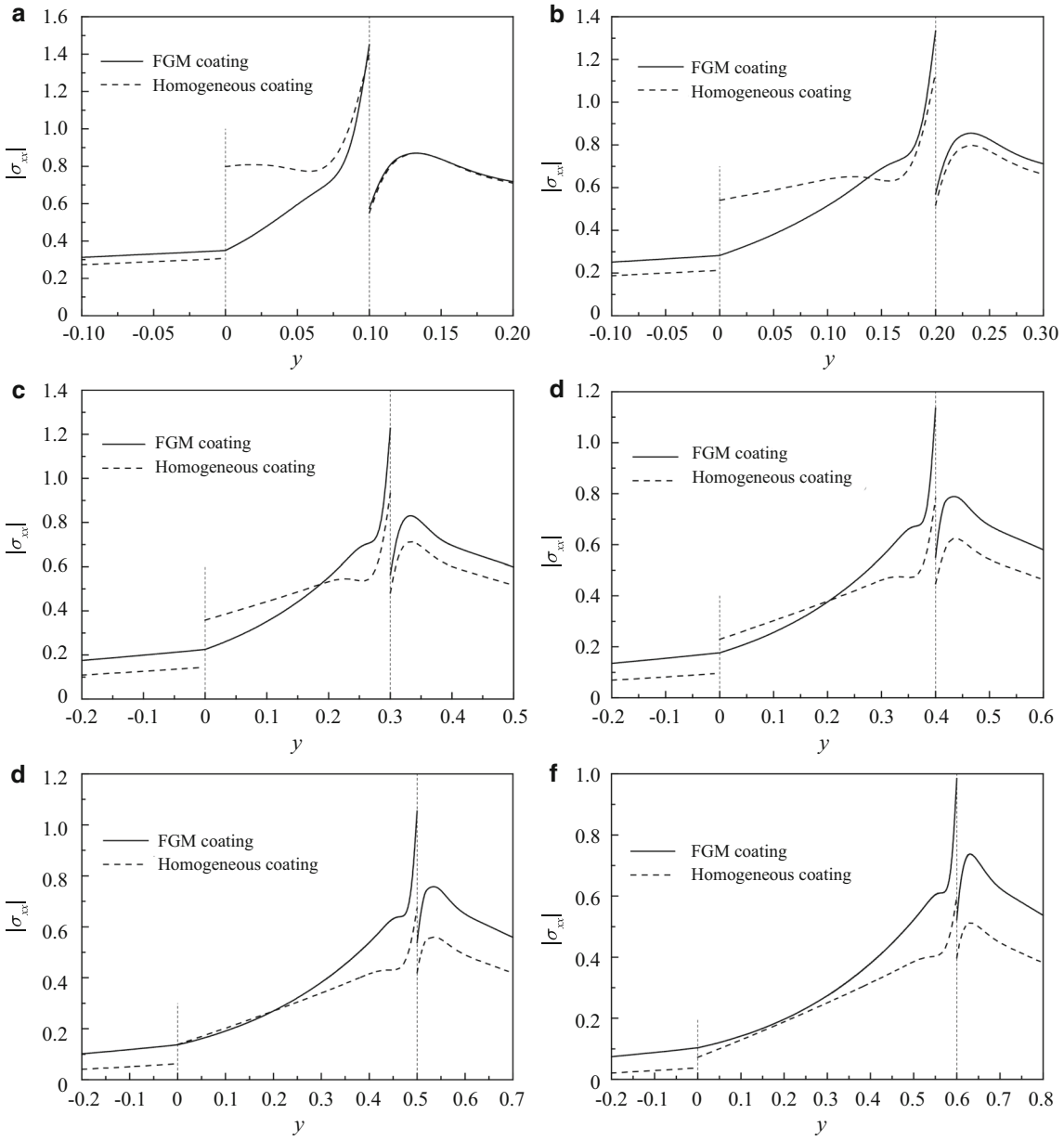

Fig. 8 Magnitude of dimensionless transverse normal stress ($|\sigma_{xx}|$) with $\psi = 0.4$: **a**–**f** $h = 0.1, 0.2, 0.3, 0.4, 0.5, 0.6$

with

$$E_0 = \mathrm{e}^{\varepsilon' y}\sum_{k=1}^{4}\left[\mathrm{i}\beta_0^2 + \left(\beta_0^2 - 2\right)a_{0k}s_{0k}\right]\left[F_{k1} - F_{k2}g_{11}/g_{12} + F_{k3}\left(\eta_{11} - \eta_{12}g_{11}/g_{12}\right)\right]\mathrm{e}^{s_{0k}y} + \mathrm{e}^{\varepsilon' y}\sum_{k=5}^{6}\left[\mathrm{i}\beta_0^2 + a_{0k}\left(\beta_0^2 - 2\right)\left(s_{0k} + \eta'\right)\right]F_{k3}\left(\eta_{11} - \eta_{12}g_{11}/g_{12}\right)\mathrm{e}^{\left(s_{0k}+\eta'\right)y} - \beta_0^2\mathrm{e}^{(\varepsilon'+\eta')y}\left(d_{05}F_{53}\mathrm{e}^{s_{05}y} + d_{06}F_{63}\mathrm{e}^{s_{06}y}\right)\left(\eta_{11} - \eta_{12}g_{11}/g_{12}\right), \tag{75a}$$

$$E_1 = [\mathrm{i}\beta_1^2 + (\beta_1^2 - 2)a_{11}s_{11}]\mathrm{e}^{s_{11}y} - [\mathrm{i}\beta_1^2 + (\beta_1^2 - 2)a_{12}s_{12}]\mathrm{e}^{s_{12}y}g_{11}/g_{12} + [\mathrm{i}\beta_1^2 + (\beta_1^2 - 2)a_{13}s_{13} - \beta_1^2 d_{13}](\eta_{11} - \eta_{12}g_{11}/g_{12})\mathrm{e}^{s_{13}y}, \tag{75b}$$

$$E_2 = \left[\mathrm{i}\beta_2^2 + \left(\beta_2^2 - 2\right)a_{21}s_{21}\right]\left(l_{11} - l_{12}g_{11}/g_{12}\right)\mathrm{e}^{s_{11}y} + \left[\mathrm{i}\beta_2^2 + \left(\beta_2^2 - 2\right)a_{22}s_{22}\right]\left(l_{21} - l_{22}g_{11}/g_{12}\right)\mathrm{e}^{s_{22}y} + \left[\mathrm{i}\beta_2^2 + \left(\beta_2^2 - 2\right)a_{23}s_{23} - \beta_2^2 d_{23}\right]\left[\eta_{21}\left(l_{11} - l_{12}g_{11}/g_{12}\right) + \eta_{22}\left(l_{21} - l_{22}g_{11}/g_{12}\right)\right]\mathrm{e}^{s_{23}y}. \tag{75c}$$

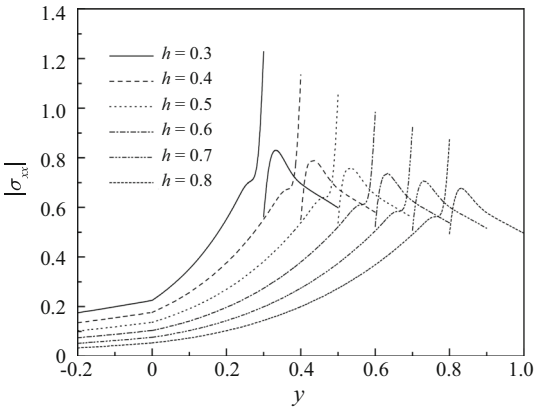

Fig. 9 Effect of dimensionless layer thickness h on the distribution of the dimensionless dynamic normal stress ($|\sigma_{xx}|$) with $\psi = 0.4$

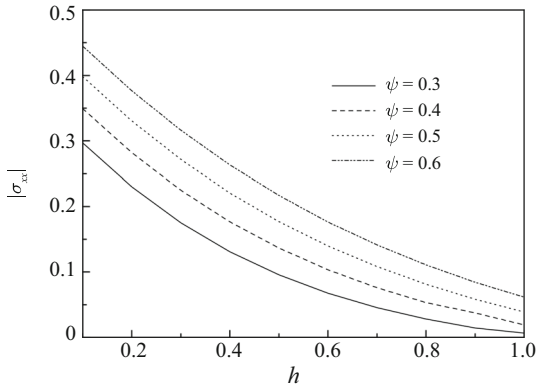

Fig. 10 Relations of $|\sigma_{xx}|$ versus h for selected values of ψ at the bonded interface $y = 0$

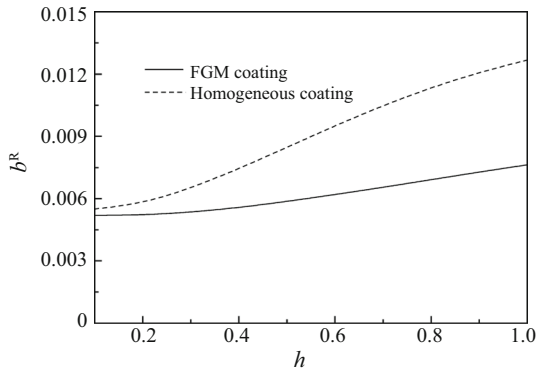

Fig. 11 Variation of the exponential growth rate b^{R} with dimensionless layer thickness h for $\psi = 0.4$

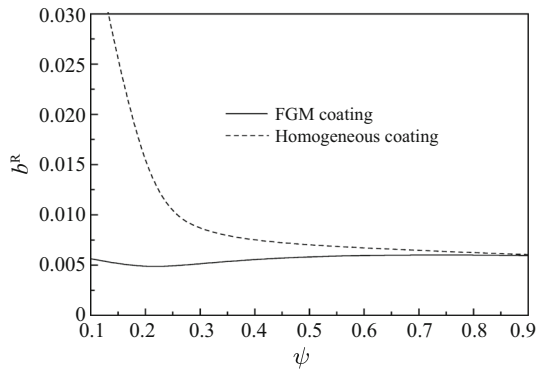

Fig. 12 Variation of the exponential growth rate b^{R} with ψ for $h = 0.4$

For the homogeneous coated structure, the results can be obtained from Eq. (74) by setting $\varepsilon' = \eta' = 0$.

The amplitudes of the dimensionless transverse normal stresses $|\sigma_{xx}|$ for the two different coated structures with a selected coating thickness are presented in Fig. 8a–e. The amplitude of the dimensionless interfacial stress is continuous at the bonded interface $y = 0$ for the FGM-coated structure, while that in the homogeneous coated structure is discontinuous because of the mismatch in materials properties between the lower half-plane and the coating. With decrease of the coating thickness, the discontinuity in the amplitude of the thermoelastic dynamic interfacial stress becomes increasingly obvious at the bonded interface $y = 0$ in the homogeneous coated structure. Furthermore, the amplitude of the thermoelastic dynamic interfacial stress in the homogeneous coated structure is lower than that in the FGM-coated structure at the sliding interface $y = -h$. This continuous and smooth stress distribution can significantly reduce the possibility of interfacial failure in the FGM-coated structure.

Figure 9 shows the relations of the amplitude of the dimensionless transverse normal stresses $|\sigma_{xx}|$ and the dimensionless layer thickness for the FGM-coated structure, revealing that the amplitude of $|\sigma_{xx}|$ decreases with increase of the coating thickness at the bonded interface $y = 0$ as well as at the sliding interface $y = -h$. At $y = 0$, the effect of the coating thickness on the distribution of $|\sigma_{xx}|$ for some selected values of ψ in the FGM-coated structure is shown in Fig. 10, revealing that the amplitude of $|\sigma_{xx}|$ decreases with decreasing value of the material mismatch parameter ψ at $y = -h$. These results indicate that the amplitude of the interface stress can be effectively reduced by changing the coating thickness properly. This is of practical importance because large tensile stress $|\sigma_{xx}|$ is the main cause of interfacial cracking.

Analysis of the stability of the two different coated structures for selected coating thicknesses are presented in Figs. 11 and 12. For the given material mismatch, b^{R} increases as the coating thickness increases for both coated structures, whereas b^{R} in the FGM-coated structure is less than that in the homogeneous coated structure, especially for large coating thickness (Fig. 11). For given coating thickness, b^{R} in the FGM-coated structure is less than that in the homogeneous coated structure, especially

for large material mismatch (Fig. 12). These results imply that the frictional sliding of the FGM-coated structure is more stable than that of the homogeneous coated structure, especially for large coating thickness and/or large material mismatch.

5 Conclusions

By considering the stability of the Adams' family wave caused by a perturbation, this paper investigates the frictionally excited TEDI of an FGM-coated structure. The thermoelastic properties of the FGM are assumed to vary exponentially with thickness. We examined the effects of the coating gradient index, sliding speed, and friction coefficient on the TEDI for various material combinations. In addition, we calculated the transverse normal stresses varying in the thickness direction for two different coating structures and analyzed the effects of the FGM coating on the stress distribution and frictional sliding stability. It is found that:

1. The exponential growth rate remains unchanged when the gradient index is less than a certain negative value. As the gradient index increases from negative to positive, the exponential growth rate fluctuates then decreases gradually to zero.
2. The results imply that one can modify the sliding stability, critical friction coefficient, and critical sliding speed by adjusting the gradient index of the FGM coating.
3. Unlike the homogeneous coating structure, the FGM-coated structure has continuous tensile stresses at the bonded interface.
4. The amplitude of the interface tensile stress can be effectively reduced by changing the FGM coating thickness properly. This means that FGM-coated structures are more effective for controlling the interfacial tensile stress. One can use this to reduce the possibility of interfacial failure.

Acknowledgements The work was supported by the National Natural Science Foundation of China (Grants 11502089 and 11725207).

Appendix

$$\eta_{1j} = \sum_{k=1}^{4} (\gamma_{1k} - f\gamma_{2k}) F_{kj} \mathrm{e}^{s_{0k}h}/\delta_k, \quad j = 1, 2, \tag{A.1}$$

$$\begin{aligned}\delta_k = & \sum_{k=1}^{4} (f\gamma_{2k} - \gamma_{1k}) F_{k3} \mathrm{e}^{s_{0k}h} \\ & - f\beta_0^2 \mathrm{e}^{\eta' h}\left(d_{05} F_{53} \mathrm{e}^{s_{05}h} + d_{06} F_{63} \mathrm{e}^{s_{06}h}\right) \\ & + \sum_{k=5}^{6}\left\{ f\left[\beta_0^2 a_{0k}\left(s_{0k} + \eta'\right) + \mathrm{i}\left(\beta_0^2 - 2\right)\right]\right. \\ & \left. -\left(s_{0k} + \eta' + \mathrm{i}a_{0k}\right)\right\} F_{k3} \mathrm{e}^{(s_{0k}+\eta')h},\end{aligned} \tag{A.2}$$

$$r_{1k} = s_{0k} + \mathrm{i}a_{0k}, \quad r_{2k} = \beta_0^2 a_{0k} s_{0k} + \mathrm{i}\left(\beta_0^2 - 2\right), \tag{A.3}$$

$$\begin{aligned} l_{1j} &= \mathrm{e}^{-\varepsilon' h} \frac{m_{1j} m_{24} - m_{2j} m_{14}}{m_{13} m_{24} - m_{23} m_{14}}, \\ l_{2j} &= \mathrm{e}^{-\varepsilon' h} \frac{m_{1j} m_{23} - m_{2j} m_{13}}{m_{14} m_{23} - m_{24} m_{13}}, \quad j = 1, 2, \end{aligned} \tag{A.4}$$

$$\begin{aligned} m_{1j} = & \sum_{k=1}^{4} a_{0k} F_{kj} \mathrm{e}^{s_{0k}h} \\ & + \left[\sum_{k=1}^{4} a_{0k} F_{k3} \mathrm{e}^{s_{0k}h} + a_{05} F_{53} \mathrm{e}^{(s_{05}+\eta')h} + a_{06} F_{63} \mathrm{e}^{(s_{06}+\eta')h}\right] \\ & \eta_{1j}, \quad j = 1, 2, \end{aligned} \tag{A.5}$$

$$\begin{aligned} m_{13} &= a_{21} \mathrm{e}^{s_{21}h} + \eta_{21} a_{23} \mathrm{e}^{s_{23}h}, \\ m_{14} &= a_{22} \mathrm{e}^{s_{22}h} + \eta_{22} a_{23} \mathrm{e}^{s_{23}h}, \end{aligned} \tag{A.6}$$

$$\begin{aligned} m_{2j} = & \left(\mu_0 / \mu_2\right) \sum_{k=1}^{4} r_{2k} F_{kj} \mathrm{e}^{s_{0k}h} + \left(\mu_0 / \mu_2\right) \\ & \left\{\sum_{k=1}^{4} r_{2k} F_{k3} \mathrm{e}^{s_{0k}h} + \sum_{k=5}^{6}\left[\beta_0^2 a_{0k}\left(s_{0k} + \eta'\right)\right.\right. \\ & \left.\left. + \mathrm{i}\left(\beta_0^2 - 2\right)\right] F_{k3} \mathrm{e}^{(s_{0k}+\eta')h}\right\} \eta_{1j} \\ & - \beta_0^2 \left(\mu_0 / \mu_2\right)\left[d_{05} F_{53} \mathrm{e}^{(s_{05}+\eta')}\right. \\ & \left. + d_{06} F_{63} \mathrm{e}^{(s_{06}+\eta')}\right] \eta_{1j}, \quad j = 1, 2, \end{aligned} \tag{A.7}$$

$$\begin{aligned} m_{23} = & \left[\beta_2^2 a_{21} s_{21} + \mathrm{i}\left(\beta_2^2 - 2\right)\right] \mathrm{e}^{s_{21}h} \\ & + \left[\beta_2^2 a_{23} s_{23} + \mathrm{i}\left(\beta_2^2 - 2\right) - \beta_2^2 d_{23}\right] \eta_{21} \mathrm{e}^{s_{23}h}, \end{aligned} \tag{A.8}$$

$$\begin{aligned} m_{24} = & \left[\beta_2^2 s_{22} a_{22} + \mathrm{i}\left(\beta_2^2 - 2\right)\right] \mathrm{e}^{s_{22}h} \\ & + \left[\beta_2^2 s_{23} a_{23} + \mathrm{i}\left(\beta_2^2 - 2\right) - \beta_2^2 d_{23}\right] \eta_{22} \mathrm{e}^{s_{23}h}. \end{aligned} \tag{A.9}$$

References

1. Suresh, S., Mortensen, A.: Fundamentals of functionally graded materials: processing and thermomechanical behavior of graded metals and metal-ceramic composites. IOM Communications Ltd., London (1998)
2. Guler, M.A.: Contact mechanics of FGM coatings. Ph. D. Thesis, Lehigh University (2001)
3. Guler, M.A., Erdogan, F.: Contact mechanics of graded coatings. Int. J. Solids Struct. **41**, 3865–3889 (2004)

4. Guler, M.A., Erdogan, F.: Contact mechanics of two deformable elastic solids with graded coatings. Mech. Mater. **38**, 633–647 (2006)
5. Guler, M.A., Erdogan, F.: The frictional sliding contact problems of rigid parabolic and cylindrical stamps on graded coatings. Int. J. Mech. Sci. **49**, 161–182 (2007)
6. El-Borgi, S., Abdelmousla, R., Keer, L.: A receding contact plane problem between a functionally graded layer and a homogeneous substrate. Int. J. Solids Struct. **43**, 658–674 (2006)
7. Elloumi, R., Kallel-Kamoun, I., El-Borgi, S.: A fully coupled partial slip contact problem in a graded half-plane. Mech. Mater. **42**, 417–428 (2010)
8. Ke, L.L., Wang, Y.S.: Fretting contact of two dissimilar elastic bodies with functionally graded coatings. Mech. Adv. Mater. Struct. **17**, 433–447 (2010)
9. Suresh, S., Olsson, M., Padture, N.P., et al.: Engineering the resistance to sliding contact damage through controlled gradients in elastic properties at contact surfaces. Acta Mater. **47**, 3915–3926 (1999)
10. Pender, D.C., Padture, N.P., Giannakopoulos, A.E., et al.: Gradients in elastic modulus for improved contact-damage resistance. Part I: the silicon nitride-oxy nitride glass system. Acta Mater. **49**, 3255–3262 (2001)
11. Suresh, S.: Graded materials for resistance to contact deformation and damage. Science **292**, 2447–2451 (2001)
12. Aizikovich, S.M., Alexandrov, V.M., Kalker, J.J., et al.: Analytical solution of the spherical indentation problem for a half-space with gradients with the depth elastic properties. Int. J. Solids Struct. **39**, 2745–2772 (2002)
13. Choi, H.J., Paulino, G.H.: Interfacial cracking in a graded coating/substrate system loaded by a frictional sliding flat punch. Proc. R. Soc. A **466**, 853–880 (2010)
14. Childlow, S.J., Teodorescu, M., Vaughan, N.D.: Predicting the deflection and sub-surface stress field within two-dimensional inhomogeneously elastic bonded layered solids under pressure. Int. J. Solids Struct. **48**, 3243–3256 (2011)
15. Aizikovich, S.M., Vasil'ev, A.S., Krenev, L.I., et al.: Contact problems for functionally graded materials of complicated structure. Mech. Compos. Mater. **47**, 539–548 (2011)
16. Comez, I.: Contact problem of a functionally graded layer resting on a Winkler foundation. Acta Mech. **224**, 2833–2843 (2013)
17. Childlow, S.J., Teodorescu, M.: Sliding contact problems involving inhomogeneous materials comprising a coating-transition layer-substrate and a rigid punch. Int. J. Solids Struct. **51**, 1931–1945 (2014)
18. Liu, T.J., Xing, Y.M.: Analysis of graded coatings for resistance to contact deformation and damage based on a new multi-layer model. Int. J. Mech. Sci. **81**, 158–164 (2014)
19. Choi, H.J., Paulino, G.H.: Thermoelastic contact mechanics for a flat punch sliding over a graded coating/substrate system with frictional heat generation. J. Mech. Phys. Solids **56**, 1673–1692 (2008)
20. Barik, S.P., Kanoria, M., Chaudhuri, P.K.: Steady state thermoelastic contact problem in a functionally graded material. Int. J. Eng. Sci. **46**, 775–789 (2008)
21. Shahzamanian, M.M., Sahari, B.B., Bayat, M.: Transient and thermal contact analysis for the elastic behavior of functionally graded brake disks due to mechanical and thermal loads. Mater. Des. **31**, 4655–4665 (2010)
22. Shahzamanian, M.M., Sahari, B.B., Bayat, M., et al.: Finite element analysis of thermoelastic contact problem in functionally graded axisymmetric brake disks. Compos. Struct. **92**, 1591–1602 (2010)
23. Chen, P.J., Chen, S.H., Peng, Z.: Thermo-contact mechanics of a rigid cylindrical punch sliding on a finite graded layer. Acta Mech. **223**, 2647–2665 (2012)
24. Chen, P.J., Chen, S.H.: Thermo-mechanical contact behavior of a finite graded layer under a sliding punch with heat generation. Int. J. Solids Struct. **50**, 1109–1119 (2013)
25. Dow, T.A., Burton, R.A.: Thermoelastic instability of sliding contact in the absence of wear. Wear **19**, 315–328 (1972)
26. Jang, Y.H., Ahn, S.: Frictionally-excited thermoelastic instability in functionally graded material. Wear **262**, 1102–1112 (2007)
27. Lee, S., Jang, Y.H.: Effect of functionally graded material on frictionally excited thermoelastic instability. Wear **266**, 139–146 (2009)
28. Lee, S., Jang, Y.H.: Frictionally excited thermoelastic instability in a thin layer of functionally graded material sliding between half-planes. Wear **267**, 1715–1722 (2009)
29. Hernik, S.: Modeling FGM brake disk against global thermoelastic instability (hot-spot). Math. Mech. **89**, 88–106 (2009)
30. Afferrante, L., Ciavarella, M., Barber, J.R.: Sliding thermoelastodynamic instability. Proc. R. Soc. **462**, 2161–2176 (2006)
31. Afferrante, L., Ciavarella, M., Barber, J.R.: A note on thermoelastodynamic instability (TEDI) for a 1D elastic layer: force control. Int. J. Solids Struct. **44**, 1380–1390 (2006)
32. Afferrante, L., Ciavarella, M., Barber, J.R.: "Frictionless" and "frictional" ThermoElastic dynamic instability (TEDI) of sliding contacts. J. Mech. Phys. Solids **54**, 2330–2353 (2006)
33. Afferrante, L., Ciavarella, M.: Thermo-elastic dynamic instability (TEDI) in frictional sliding of a half plane against a rigid non-conducting wall. J. Appl. Mech. **74**, 875–884 (2006)
34. Afferrante, L., Ciavarella, M., Barber, J.R.: Thermo-elastic dynamic instability (TEDI) in frictional sliding of two elastic half-spaces. J. Mech. Phys. Solids **55**, 744–764 (2007)
35. Liu, J., Wang, Y.S., Ke, L.L., et al.: Thermo-elastic dynamic instability of an elastic half-plane sliding against a coated half-plane. Int. J. Mech. Sci. **117**, 275–285 (2016)
36. Liu, J., Wang, Y.S., Ke, L.L., et al.: Dynamic instability of an elastic solid sliding against a functionally graded material coated half-plane. Int. J. Mech. Sci. **89**, 323–331 (2014)
37. Mao, J.J., Ke, L.L., Wang, Y.S.: Thermoelastic contact instability of a functionally graded layer and a homogeneous half-plane. Int. J. Solids Struct. **51**, 3962–3972 (2014)
38. Mao, J.J., Ke, L.L., Wang, Y.S.: Thermoelastic contact instability of a functionally graded layer interacting with a homogeneous layer. Int. J. Mech. Sci. **99**, 218–227 (2015)
39. Hills, D.A., Baber, J.R.: Steady motion of an insulating rigid flat-ended punch over a thermally conducting half-plane. Wear **102**, 15–22 (1985)